International Journal of Astrophysics and Space Science
2026, Vol. 14, No. 3, pp. 69–81
https://doi.org/10.11648/j.ijass.20261403.13

Research Article

Single vs Double Asteroids, DART Mission, and Space Trajectory Analysis Mapping

Kolemann Lutz*

Earth and Planetary Science Department, MultiPlanet University, Washington, United States

Abstract

Since 1900s humans have believed in hypothetical binary asteroids with 16% of Near Earth Asteroids (NEAs) proposed to be binaries or 6,400 binary asteroids proposed since 1993. This research study is one of first to classify asteroids as single body systems and how light refraction angles-ecc similar to a 33min variance may not be sufficient to justify post-impact trajectory dV. This R&D would revise 600 asteroids identified and update <6,000+ binaries orbits, sizes, and estimates in databases. Study conducts radar, optical lightcurves analysis, time series analysis, Pixel data analysis, aberrations, and finds cloned asteroid data. ESA HERA $440M Mission was designed to investigate moonlet vs Didymos. This R&D Analysis may update $440m DART and HERA Mission, Software FSW, C&DH, TCM Orbits, to successfully image collect data of asteroids and extend Mission CONOPs applied to nearby asteroids objects. This research may significantly update 6,400+ asteroids in databases, telescope observation surveys, trajectory FSW, data analysis methods of pre-post impact orbits with new trajectories. This research could recover billions of dollars in operations and space missions to advance planetary science, defense, missions, and beyond.

Keywords

Astrophysics, Planet Defense, Space Science, Mission Engineering, Optics, Flight Software

1. Background

After a Mars flyby in March 2025 and a deep space maneuver in February 2026, a six-month survey of asteroid Dimorphos with 11.5m solar arrays is planned. Dimorphos, is believed to be "moonlet" 160m orbiting Didymos, believed to be 780m, 2.5X taller than Eiffel Tower, orbiting Elliptical 1-2.3AU.

620 have been discovered multiple-system asteroids Near-Earth Asteroids (NEAs) with 15-17% as 112+ systems Main Belt Asteroids (MBAs), 6% (higher for small sizes) 322+ systems. Trans Neptunian (TNO) asteroids are 20-30% theorized to be binaries with asteroids from [4].

*Correspondence: Kolemann Lutz (kole@mp-university.net)

Received: 14 June 2026; **Accepted:** 30 July 2026; **Published:** 28 September 2026

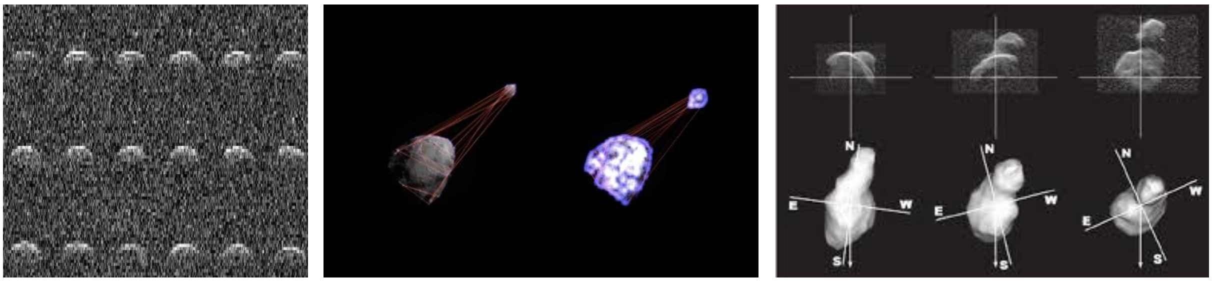

Figure 1. a) Example of Binary Asteroid Radar data, b and c) Dart Mission Proposed as Binary with similarity, details, clusters of cloned pixels similar sizes from APL DART Youtube Video, 2023.

Asteroid Population	Theoretic / Estimated Binary Fraction	Found / Confirmed Binaries	Estimated Total Single Asteroids
Near-Earth Asteroids (NEAs)	~ 15% – 17%	112+ systems	~ 30,000 discovered
Main Belt Asteroids (MBAs)	~ 6% (higher for small sizes)	322+ systems	~ 1.3 million known
Jupiter Trojans	~ 10% – 23%	8 systems	~ 7,000 known
Mars Crossers	Unknown / Varies	36+ systems	~ 25,000 known
Trans-Neptunian Objects (TNOs)	~ 20% – 30%+	149+ systems	~ 3,000 + discovered
Total Companions	-	650 total known	Millions (over 1.5 million known overall)

Figure 2. NEA Binaries vs Single estimates and b) Binary Asteroid Optical Data Example.

Asteroid binaries were primarily proposed through three methods: Lucky Spacecraft flybys, ground-based lightcurve analysis measuring periodic eclipses, and high-resolution radar imaging. Ground based telescopes also noticed periodic, tiny dips in brightness, which were caused by one asteroid eclipsing or casting a shadow over the other High-res radar mapping (bouncing radio waves off asteroids) allowed astronomers to map shapes of bodies.

The first binary asteroid system ever detected was discovered using planetary radar at NASA's Goldstone tracking facility in California. Since then Arecibo Observatory has been a primary to discover binary asteroids. NSF funded, Cornell then later UCF Managed based in Puerto Rico is owned by NSF facility confirmed 60 multiple asteroid systems, or about 73% of known multiple near-Earth asteroid systems. However, 305-meter telescope collapsed in 2020 reconstructed with Aracebo. Ida was accompanied by a tiny moon, Dactyl, first proposed satellite of an asteroid.

2. Methods

2.1. Delay-Doppler Radar, Optical Lightcurves Analysis

Doppler RF antenna works based on time delay or distance to the target. Delay-Doppler Map (DDM) measures the distribution of echo power returned. The plotted values in the map (often in Watts are converted to dB for a wider dynamic range) are typically echo powers detected by the receiver. The power in Watts in Delay-Doppler pixel is determined by several core factors: Target Reflectivity (RCS): radar cross section SD, system power gain spread function or PSF Jacobian. The radar albedo depends on the near-surface electric permittivity of the target, which itself depends on the near-surface mineralogy, density, and the volume fraction of metals [3, 17].

Doppler frequency shift (velocity of the target) is based on Orthogonal Time Frequency Space (OTFS). First echoes to arrive come from the closest parts of the asteroid, while later echoes come from the most distant parts, which is suggested to measure depth and size. Delay -Doppler Domain: Maps channel changes into stable, separable coordinates. Radio transmits and records how long the echo takes to bounce back, as Doppler effect frequency shift can quantify relative velocity. Characterizing these objects, astronomers pair optical lightcurves with delay -Doppler radar. Radar imaging is crucial for planetary defense because it enables ultra-precise range and velocity measurements to define near-Earth collision probabilities, Data synthesized from [12, 19]. OTFS maps reflections into a localized Delay-Doppler (DD) grid. Because the entire signal experiences the same Doppler shift, it eliminates Inter-Carrier Interference (ICI). OTFS is inter-carrier interference-free and can accurately measure Doppler frequencies is up to full subcarrier spacing vs OFDM limited to detecting about 10%.

2.2. Binary Asteroid NEO Detection Analysis and Telescope Observation Methods

12 highly-characterized binary Near-Earth Asteroids (NEAs)				
	Diameter (km)	Companion Diameter (km)	Primary Reference Dataset / Telescope Observatory	Notes / Link
(65803) Didymos	0.78	0.16	Arecibo Observatory , Goldstone, DART/Hera	Minor planet binary system.
(66391) Moshup	1.31	0.45	Goldstone Solar System Radar	Better known as 1999 KW4.
(185851) 2000 DP107	0.8	0.3	Arecibo, Goldstone	Classic contact binary system primary.
(276049) 2002 CE26	3.5	0.8	Arecibo Observatory , Lowell Obs	Exceptionally large primary for an NEA binary.
(164121) 2003 YT1	1.1	**0.16**	Goldstone, Arecibo	Well-studied triple/binary NEA.
(88710) 2001 SL9	1.18	0.31	Arecibo, Goldstone	Rapid rotator, tidally locked.
(35107) 1991 VH	1.2	0.3	Arecibo, Goldstone	Prominent radar target.
(136617) 1994 CC	0.6	0.15	Arecibo, Goldstone, MIT	Triple system with inner/outer moons.
(153591) 2001 SN263	2.6	1	Gemini Observatory , Arecibo	Large ternary NEA system.
(175706) 1996 FG3	1.4	0.45	European Southern Observatory , Goldstone	Favorable for spin-state studies.
(363505) 2003 UC20	0.6	0.15	Arecibo, Goldstone	Radar-discovered companion.
(308635) 2005 YU55	0.4	0.1	Arecibo, Goldstone	Subject of intense flyby observations.

Observation Method	Capability & KPI Impact	Limitations
Radar Delay-Doppler	Provides line-of-sight range (distance) and velocity (Doppler frequency) with resolutions down to ~ 1.875 meters/pixel. Constrains binary orbit, sizes, spin states, and sub-surface properties.	Requires close proximity to Earth; transmitter power drops rapidly with distance (r^4 law).
Optical Astrometry	Excellent for early discoveries and measuring angular positions on the sky plane.	Poor at defining exact line-of-sight distance; uncertainties grow rapidly with time.
Optical Photometry (Lightcurves)	Determines rotation periods, binarity fractions via mutual eclipses/transits, and satellite-to-primary ratios.	Less accurate for sizing objects without albedo estimations, and does not yield precise ranging for orbit refinement.
Infrared Spectroscopy	Characterizes composition (e.g., C-class, S-class) and thermal albedo.	Provides little data on orbital dynamics, trajectories, or collision geometries.

Target Object	Estimated Diameter (km)	Radar Cross Section (RCS)	Primary Observation / Discovery Method	Key Physical KPI (Period / Density)	Associated Danger Level
66391 Moshup (1999 KW4)	1.3 (Alpha), 0.4 (Beta)	0.84 km^2	Radar Delay-Doppler & Opt	2.8h (Alpha), 17.4h (Beta) / 1.9 g/cm^3	PHA, High AI
80976 (2000 UG58)	~1.2 (Alpha), ~0.4 (Beta)	~0.60 km^2	Radar Delay-Doppler	System Orbit: 12.5 days	Potentially Hazardous Asteroid (PHA)
(185851) 2000 DP107	~0.8 (Primary)	~0.30 km^2	Opt Lightcurve + Radar Delay	Orbit: 1.76 days / Dens: 1.4 g/cm^3	PHA
1994 CC	~0.6 (Primary), ~0.07 (Sec.)	~0.15 km^2	Radar delay-Doppler / Bistatic	12.2h (Pri), 27.5h (Sec) / 1.5 g/cm^3	PHA, Triple System
2003 YT1	~1.1 (Pri), ~0.15 (Sec.)	~0.55 km^2	Radar Delay-Doppler	1.9h (Pri), 36.7h (Sec) / 2.0 g/cm^3	PHA
(3122) Florence	4.5 (Primary), 0.3 (Two moons)	4.2 km^2	Optical & Radar Delay-Doppler	2.4h (Pri), 22h/27h (Moons)	PHA, Earth Close Pass

Figure 3. *a) PHA's Detected and Observation Methods with KPI's from Observatories i.e. Arecibo. Characterized binary (NEAs) noting primary facilities observatories proposing binaries from Arecibo, Goldstone in Puerto Rico, Goldston DSN Green Bank, HST, Vera Rubin.*

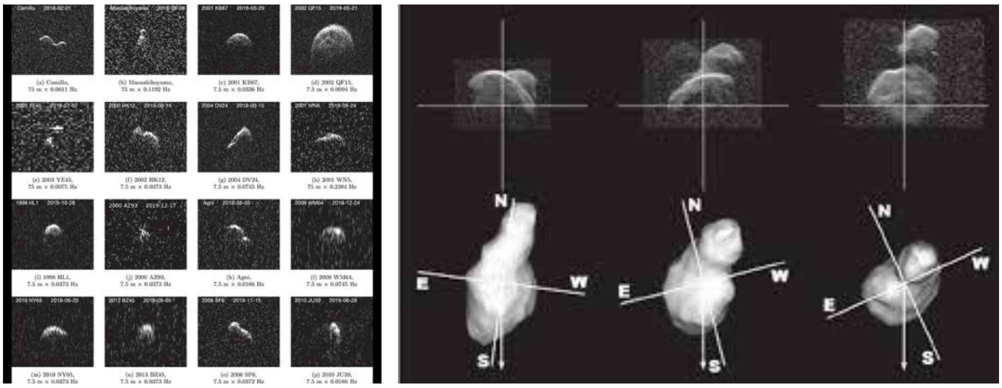

Figure 4. *Radar Delay-Doppler images of NEA's (Virkki et al. 2022). Credit: The Planetary Science Journal (2022). b) Radar Astronomy Delay Doppler, [13].*

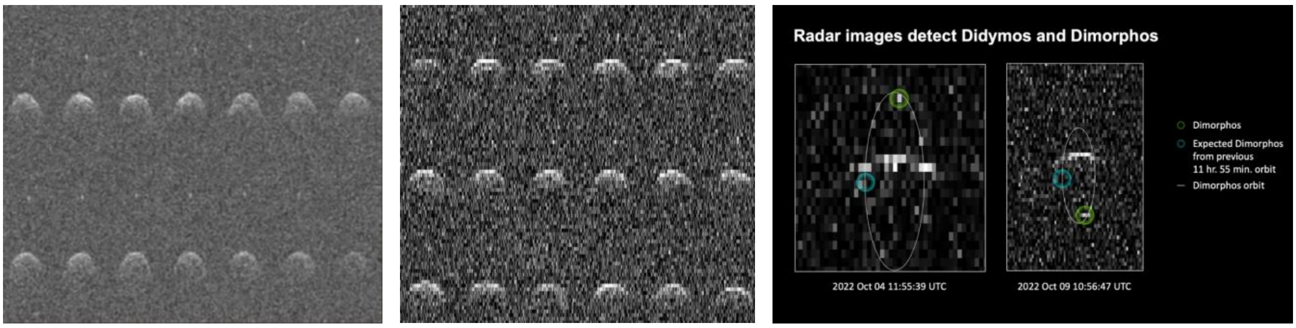

Figure 5. *a) Arecibo vs Goldstone delay -Doppler images of Didymos obtained on 2003 Nov 14-15 .5us x .5Hz time delay downward. [8].*

Each image is a sum of three runs, during which the primary rotated about 11deg in bottom and authors claim asteroid rotated 17deg in top. However, note the proposed bright pixel or interpreted as a natural satellite remains primarily fixed static without similar rotation. Arecibo Speckle and Phase Noise (2380 MHz, 12.6 cm) and Goldstone (8560 MHz, 3.5 cm). Delay doppler provided range resolutions of up to 15 m/ pixel that placed hundreds of pixels on the primary. System has S- and X-band radar albedos of 0.20 and 0.30 respectively, and an optical albedo of 0.15 [9]. The team also assessed how many of these asteroids are contact binaries. Found about double the expected number of contact binary asteroids, which are peanut or bowling-pin-looking asteroids with two lobes attached to each other by a neck.Conclusion came from the radar properties of binary, suggesting more of an elongated orbit around the sun, however, longer observation arcs may suggest varying eccentricities.

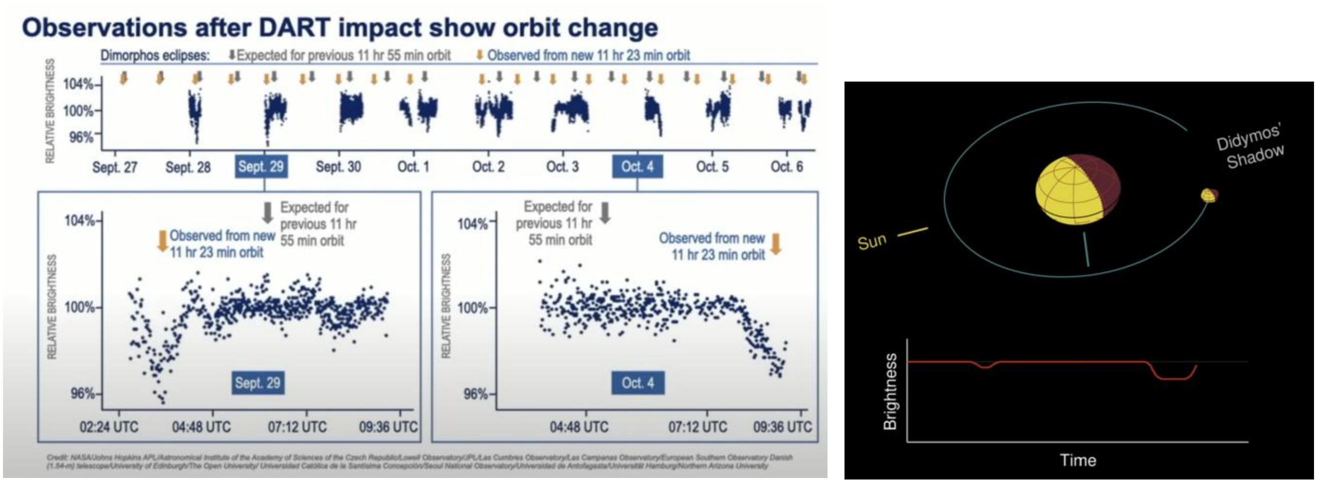

Figure 6. a) Observation after DART Impact. Expected for 11 hr 55 min to observed new 11 hr 23 min orbit and b) Shadow Brightness Deviance Illustrating 160-m asteroid may not cause much change dM, dm.

The DART mission proposes impact of Didymos in 2022 reduced the orbital period by 30min to 11hrs 23 minutes. However, a 4-6% relative change in dm for apparent magnitude, dM for absolute magnitude does not justify orbital period estimates. Also considering size of rocks with 20% Dimorphos/Didymos. Moreover, President of the Italian Space Agency that built LICIACube mentioned cubesat captured more than 700 images from Didymos system. plumes of debris are assumed from white optical lines on lens in heavily processed image from LICIA Cube optics.

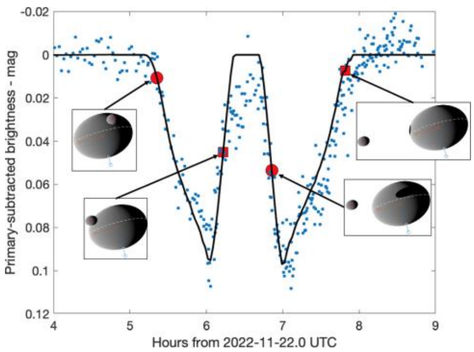

Table 2. Comparison between Naidu et al. (2020, 2022), Scheirich et al. (2024), and JPL 547

Parameter	This Paper	Scheirich et al. (2024)	Naidu et al. (2020)	Naidu et al. (2022)
λ (deg)	310 ± 3	310.0 ± 5.0	See note	310 ± 15
β (deg)	−80.7 ± 0.5	−80.4 ± 0.6	−89 ± 10	−76 ± 4
a/a_A	3.02 ± 0.08	2.92 ± 0.07	3.01 ± 0.2	Not estimated
a (km)	1.189 ± 0.017	1.150 ± 0.03	1.19 ± 0.03	1.2 (see note)
$\dot{n}$ (rad s^{-2})	$(4.8 \pm 0.6) \times 10^{-18}$	$(4.6 \pm 1.2) \times 10^{-18}$	Not estimated	$(5 \pm 1) \times 10^{-18}$
P_{imp-} (hr)	11.921493 ± 0.000016	11.92149 ± 0.00003	11.93 ± 0.01	11.921487 ± 0.000028
P_{imp+} (hr)	11.377 ± 0.004	11.3751 ± 0.0017	...	...
P_{∞} (hr)	11.3674 ± 0.0004	11.3675 ± 0.0004	...	...
$\dot{\varpi}$ (deg day^{-1})	6.7 ± 0.2	7.3 ± 0.7	...	...

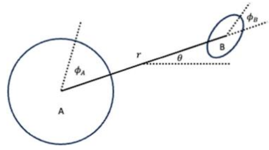

Figure 7. Photometric measurements (dots) from Moskovitz et al. [8] of a primary occultation (left minimum) and primary eclipse (right minimum) b) Comparison from Naidu, et al 2024,[9], [10], Scheirich et al. [15], and JPL 547 c) Figure. Two-body problem from Scheeres.

Red circles (squares) show the times when the COM of Dimorphos, or the COM shadow, entered (exited) the mutual event. Inset figures show system configuration corresponding to event start and stop times.

To evaluate the daily frequency and structural profile of U- and V-shaped light flux changes in binary Near-Earth Objects (NEOs), we must analyze the coupling between the system's intrinsic orbital inclination i and its geocentric Declination angle (DEC) at observation time. While the satellite's mutual orbital period sets the maximum theoretical event frequency, the instantaneous viewing geometry—defined by the asteroid's celestial coordinates (RA/DEC) relative to its binary orbital pole—determines whether eclipses are fully realized, grazing, or completely absent.

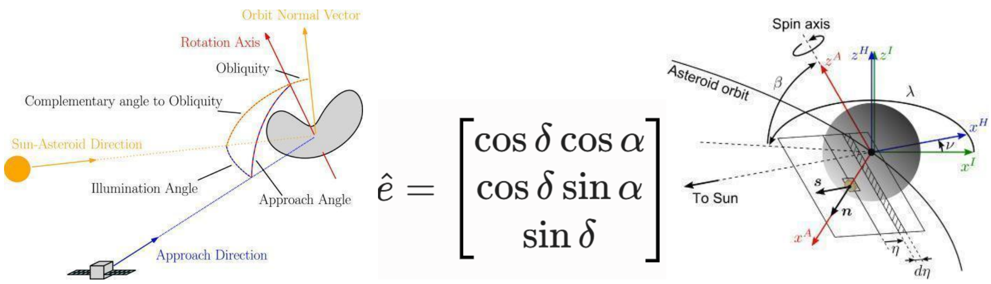

Figure 8. *Observer-to-Asteroid Vector e Defined by the asteroid's current Right Ascension (α) and Declination (δ or DEC) b) Asteroid Equations, c) Orbit angles and sun reflection vs orbit planes. C) [21].*

$$\cos\theta = e \cdot n = \cos\delta \ \cos\ \delta\ \cos\ (\alpha - \alpha_p)$$

Mutual events occur if the Earth passes close enough to the system's orbital plane based on cos θ <. For a telescope or radar station to detect a daily U- or V-shaped flux drop, the aspect angle should satisfy the geometric boundary condition for at least a partial eclipse:

$$\cos\theta < \frac{Rp+Rs}{a}$$

$$V^2 = GM$$

$$V^2=GM(2/r - 1/a)$$

Vis-Viva Equation (Orbital Velocity) is proposed to help calculate scalar velocity (v) of an asteroid at any given distance (r) from the central body, where v is velocity of orbiting body at distance r, G gravitational constant, M is mass of central body, r is distance between centres of bodies, and a is semi major axis.

Mutual events of Dimorphous Orbit Determination total change of the orbital period was −33.240 ± 0.072 minutes (all uncertainties are 3σ) estimated from Scheirich et al 2024. We obtained the eccentricity of the postimpact orbit to be 0.028 ± 0.016 and the apsidal precession rate was 7.3 ± 2.0 degrees day−1 from impact to 2022 Dec 2. The data taken later in 2022 Dec to 2023 Feb suggest that eccentricity dropped close to zero or the orbit became chaotic est 70 days after impact. [15]

Potential Doppler Error Sources include grid mismatch, range folding, noise environment interference, antenna vehicle motion and other sources. Fractional delay/Doppler leads to grid mismatch errors, if not mathematically corrected (e.g., using pulse compression or joint-estimation algorithms). Range Folding: Echoes from a previous radar pulse can return after the next pulse has been transmitted, creating "second-trace echoes" that appear to be much closer to the radar than they actually are. Noise / Environment errors, Clutter & Interference: Returns from the ground, sea, or atmospheric clutter can obscure real targets or produce misleading Doppler velocity signals. Antenna/Platform Motion involves if the radar itself is moving (e.g., on an aircraft, drone, or satellite), any errors in estimating the platform's own velocity or pitch/roll will introduce systemic biases into the final delay-Doppler calculations.

Moreover, with Although with Arecibo, Apparent Size/Radius Underestimation suggest Studies comparing Arecibo synthetic models to real observations show that visual inspection alone can cause radius underestimates by roughly 20% to 45%. [20]. To execute this Radar image analysis programmatically, you would typically pass the images through a speckle filter (such as a Lee or Frost filter) to isolate the multiplicative noise, and then perform a spectral analysis on the background regions to quantify the phase noise floor before calculating the residuals.

2.3. Radar Backscatter Off Angle Collection Analysis, Normalizations

Causes and solutions from potential sources of error involve off-angle collection. Geometric Backscatter Normalization, Target Reflectivity (RCS) with specialized algorithms (such as the OSOD or delay -Doppler processing software with phase alignment.

This specific measurement geometry dictates the incidence angle or grazing angle at which the microwave signal strikes and reflects off the target surface. Depending on how the radar wave interacts with the target and the angle of obliquity, the following may be encountered:

Off-Nadir Imagery (or Oblique Viewing): The standard process of tilting a satellite sensor away from the vertical axis to broaden ground coverage, capture stereo images, or eliminate sun glint. [1, 2]

Over-The-Horizon (OTH) Radar: A specialized defense application that bounces high-frequency (HF) waves off the ionosphere at extreme off-nominal angles to detect targets thousands of miles beyond the Earth's curvature. *Geometric Backscatter Normalization:* Raw echoes are normalized to account for the angle of incidence between the radar beam and the asteroid's surface. [1] *Radar Albedo Calculation:* The received signal (radar cross-section) is normalized by the target's geometric projected area to determine the *radar albedo*. This allows scientists to compare the surface roughness and porosity across different asteroids without being skewed by the object's physical size.

To normalize this data, astronomers use specialized algorithms (such as the OSOD or delay-Doppler processing software) to perform *Coordinate Transformation:* The delay-Doppler values are projected into an *asteroid-centric coordinate system*. This normalizes the data against the specific geometry of Earth, the Sun, and the asteroid's orbit at the exact time of the observation. [1, 2] *Phase Alignment:* By combining multiple observations taken over consecutive days (known as rotational phase coverage), scientists account for the changing sub-Earth latitude.

Large-scale surveys like ATLAS and Gaia normalize hundreds of thousands of observations using IAU \(H, G, G) or \(H, G) phase functions and shape-based inversion algorithms.

Dataset Volume: Applied to millions of individual sparse photometric points and multi-epoch light curves (e.g., >300,000 asteroid records) to correct for changing Sun-asteroid-observer geometries. [22] Angular Deviations: Any observation outside the strict opposition surge region (.5-2deg) or high off-angle viewing lines introduces considerable photometric or radar backscatter distortion. Magnitude-Phase Functions: Employs IAU-standard bi-parameter (\(H, G\) to correct to absolute magnitude (H). Empirical Debiasing Schemes: Modern algorithms (like DePhOCUS) reduce residuals in massive astrometric catalogs by mapping non-linear scattering variations across varied viewing angles.

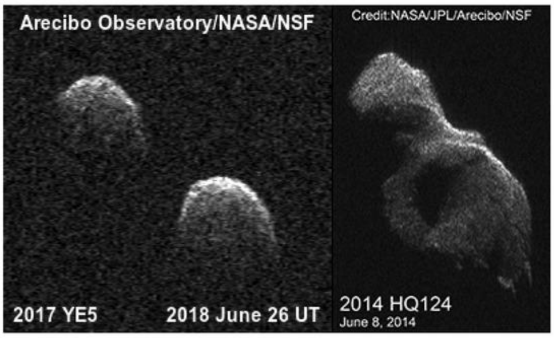

Figure 9. *Two typical high-quality delay–Doppler images of asteroids 2017 YE5 obtained using Arecibo S-band radar system (on the left) and 2014 HQ124 from bistatic X-band (Virkki, 2023).*

Common Normalization Algorithms:

1) Cosine-Square / Lambertian Correction: Traditional optic-based approximations correcting power-drop off relative to incidence angles. [23]
2) Angular Response Function (ARF) Modeling: Empirically or physically fitting backscatter intensity curves against local incidence angles to flatten range illumination biases. [23]
3) Histogram Matching / Inverse Profiling: Normalizing off-nadir swaths to match a reference incidence angle baseline via statistical distribution adjustments. [25, 26]

2.4. Dydmos Asteroid, Dart Mission Analysis

DART (Double Asteroid Redirection Test) successfully impacted the asteroid moon Dimorphos on September 26, 2022. The 610-kilogram spacecraft struck the 170-meter asteroid at a hypervelocity of approximately 6.2km/s. Asteroid system 65803 Didymos (780 m-diameter mountain-sized) was believed to have a moonlet, Dimorphos. The DART mission from JH APl claims that the impact in 2022, reduced the orbital period from 11hrs 55min to 11 hrs 23 minutes, where as some suggest high estimat.

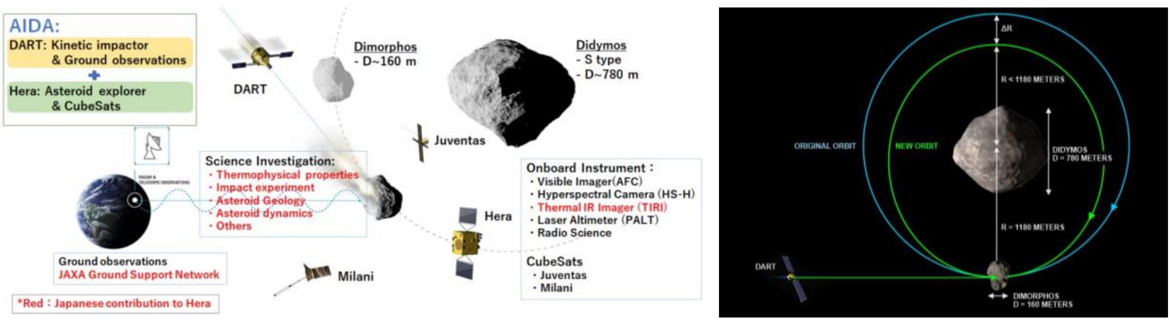

Figure 10. *DART-HERA Missions, Instruments and Orbits with analysis from a few that proposed Dimorphos with 163 m mean diameter.*

DRACO Optimal Camera derived from the Long Range Reconnaissance Imager (LORRI) camera originally built for the New Horizons mission. The DART mission missed almost 50% of time With 20um difference, where some at APL also proposed looking at a potential tertiary system Based on star tracker, A Photonic Mixer Device (PMD), While not the primary imager, research involving DART and similar rendezvous missions frequently discusses PMD (or Time-of-Flight) sensors to calculate distance and create depth maps, aiding in GNC tracking. For GNC & TT&C, engineers said they did not need reaction wheels. For rendezvous POD, Non maneuvers T-2hrs out 800km out TGO. Ejecta proposed to be from streamers below in images.

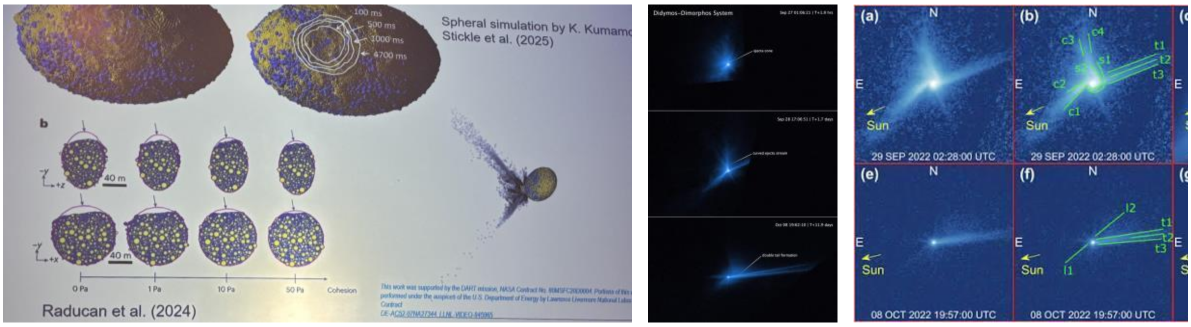

Figure 11. *HST Images from Jian-Yang Li with 63 DART Team Members, Li, 2022 and b) proposed Dimorphos Ejecta proposing thousands km long debris trails and a very weak, rubble-pile asteroid, (Ferrari, 2025).*

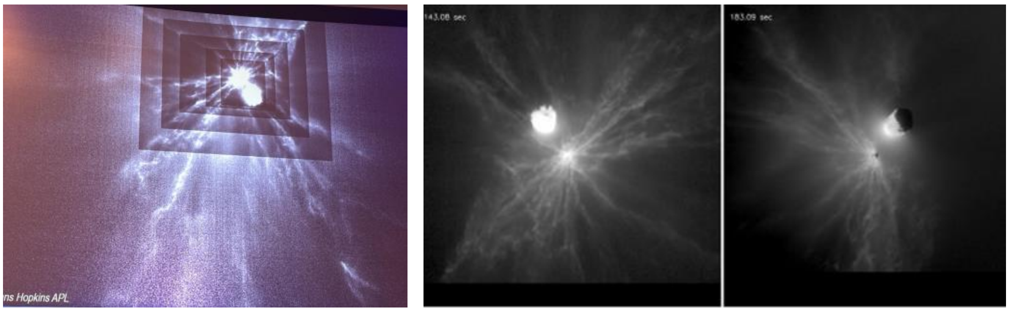

Figure 12. *DART Images from APL who proposed Ejecta is from streamers in images vs Optics Artifacts.*

The proposed collision was believed to have ejected over 1 million kgs (2.2M lbs) of rock and dust into space, creating a debris tail over 10,000 kilometers long. Rotation: asteroid likely entered a "chaotic tumbling" state rather than tidally locked However, based on Video Data, even if Two asteroids, exists, NEA Data Analysis suggests if traveling 6-7km/sec DART velocity from T-2min to Impact from Asteroid 1 to 2 suggests a separation distance of 720km - 840km, almost half US East Coast distance.

Image Orbit Impact Data Analysis. Images claimed a 10microns orbit difference and some suggest impact may have altered the asteroid into a different tumble. Some claim the orbit shrank however, if AoA was not facing sun beta angle (based on optical cameras) this may suggest alternate orbits. However, the 45min object could not be resolved based on a live dart cam, although Dimorphos looked similar in size. With T-15-25min, approaching rocks with higher velocity, DART impacted in a retrograde orbit. This means the spacecraft and the asteroid were traveling in opposite directions, resulting in a head-on collision at 6km/s about 11 million km out from Earth. With Didymos (Asteroid orbiting prograde counterclockwise), Left hand rule suggests thumb with solar velocity vector with further geometrical analysis).

Dimorphos was initially thought to be detected with Discovery Telescope (Optical) 0.65-m Telescope and with Confirmation Telescope (Radar) at Arecibo monitor the brightness of the asteroid Didymos. He noticed the periodic "dips" in light (the light curve) "detect" the moonlet inside that single dot, astronomers used a technique called Photometry (Light Curve Analysis). The Asteroid system appeared as one cluster with a small cluster of bright pixels on a digital sensor (CCD). After analyzing thousands of images, researchers initially interpreted dRGB as occultated two bodies. By plotting this brightness over time, a Light Curve brightness was proposed to dip slightly.

Figure 13. Images of the debris tail of DART impact, second tail twin believed to be from solar radiation, where it's unclear how a 2nd tail would form 7days later (NASA, ESA, 2022) from Jian-Yang Li (PSI), Joe Depasquale (STScI).

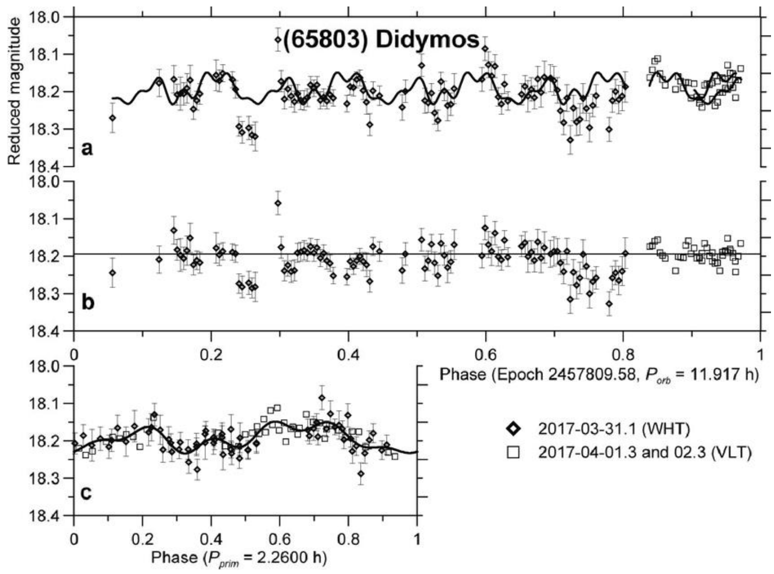

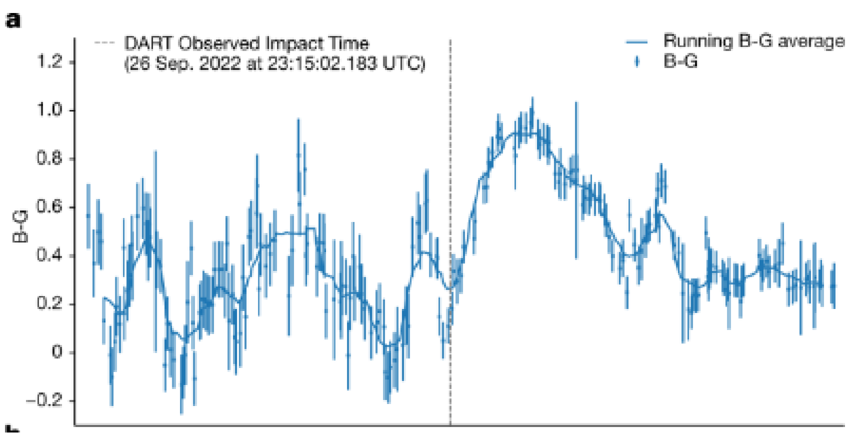

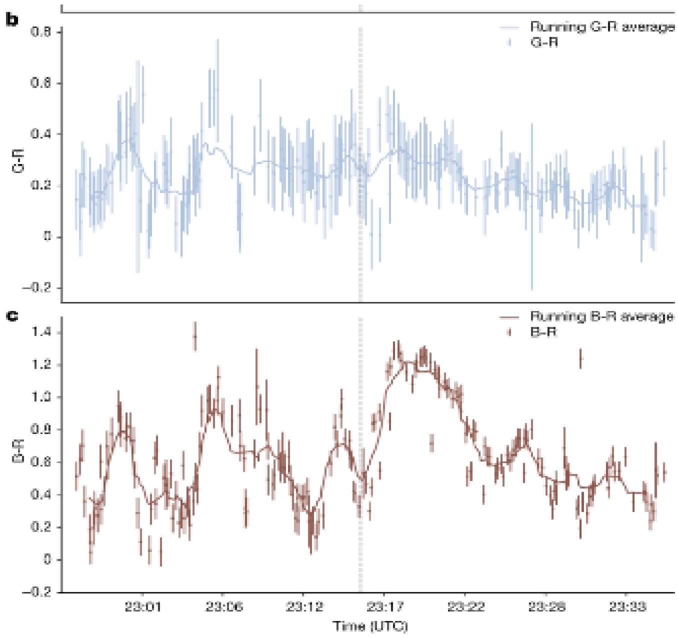

Figure 14. *Light curves and colours of the ejecta from Dimorphos after Impact.*

Graykowski, et al, 2023 estimates optical observations of Dimorphos before, during and after the impact, from a network of citizen scientists' telescopes across the world. We find a maximum brightening of 2.29 ± 0.14 mag on impact. Didymos fades back to its pre-impact brightness over the course of 23.7 ± 0.7 days. [2]

2.4. Binary PHA Analysis, Observations, Observatory Analysis

First Binary asteroid Ida asteroid and its moon Dactyl as photograph by the Galileo spacecraft (NASA, August 28, 1993).1993 The Flyby: Galileo approached within 1,500 miles (2,400 km) of Iactyl was proposed Dactyl: Measuring just 1.6 kilometers across, the little moon orbits roughly 53 miles (85 km) away from Ida. The Galileo probe didn't "know" Dactyl was there during the 1993 flyby. It used its Solid State Imaging (SSI) camera to automatically track and photograph the asteroid Ida. Months later, scientists back on Earth discovered the tiny moon Dactyl hiding in the high-resolution mosaic frames. Ida was proposed as 60x25x18km vs 1km Dactyl. Tiny moon Dactyl was discovered by Ann Harch, an assistant science coordinator on the Galileo imaging team at Cornell University. She discovered the moon on February 17, 1994, on August 28, 1993, NASA's Galileo spacecraft successfully flew by the main-belt asteroid 243 Ida while en route to Jupiter. passing 1500mi from the surface. As part of a 30-frame mosaic designed to image the asteroid itself, this frame fortuitously captured the previously unknown moon at a range of about 3,900 kilometers (2,400 miles), just over 4 minutes before closest approach to Ida.

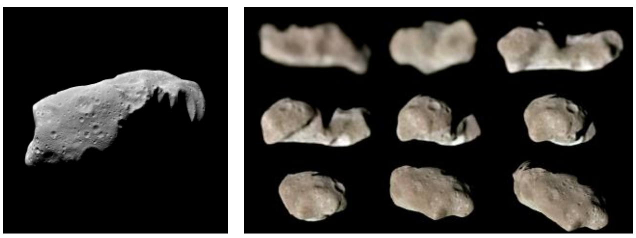

Metric	30-Frame Search Mosaic	5-Frame Target Mosaic
Capture Distance	Captured earlier at **3,900 km** out.	Captured late at **10,500 km** out.
Single Frame Size	**31.6 km × 31.6 km**	**85.1 km × 85.1 km**
Total Mosaic Footprint	**88.5 km × 149.7 km**	**73.3 km × 201.6 km**
Image Resolution	Roughly **38 meters/pixel**	Roughly **106 meters/pixel**

Figure 15. *Five-Frame Mosaic vs 30 Frame Mosaic (PIA00135) Purpose: Acquired at ranges of 3,057 to 3,821 kilometers (about 3.5 minutes before closest approach), 31-38m/pixel.30-Frame MosaicPurpose: sequence was taken a few minutes prior to closest approach..*

The 30-36 frame sequence was designed to cover a wide enough area. Rellying on low gain antenna, early data transmissions featured only these narrow, high-resolution snapshots of Ida, which is why Dactyl was completely absent. The 30-frame mosaic covered a search area roughly 6.5 times wider than the 5-frame mosaic to compensate for ephemeris uncertainties. This mosaic was structured in a grid pattern to account for wide positional errors (ephemeris uncertainties). sweeping 1.3deg x 2.2 deg or sky area of 2.86 square deg vs 5Frame .4x1.1deg or .44 square deg. An 800x800 pixel CCD sensor suggests 2.09" /pixel. Dactyl was thoroughly cross-examined across 47 separate exposures.

12 highly-characterized binary Near-Earth Asteroids (NEAs)				
	Diameter (km)	Companion Diameter (km)	Primary Reference Dataset / Telescope Observatory	Notes / Link
(65803) Didymos	0.78	0.16	Arecibo Observatory , Goldstone, DART/Hera	Minor planet binary system.
(66391) Moshup	1.31	0.45	Goldstone Solar System Radar	Better known as 1999 KW4.
(185851) 2000 DP107	0.8	0.3	Arecibo, Goldstone	Classic contact binary system primary.
(276049) 2002 CE26	3.5	0.8	Arecibo Observatory , Lowell Obs	Exceptionally large primary for an NEA binary.
(164121) 2003 YT1	1.1	**0.16**	Goldstone, Arecibo	Well-studied triple/binary NEA.
(88710) 2001 SL9	1.18	0.31	Arecibo, Goldstone	Rapid rotator, tidally locked.
(35107) 1991 VH	1.2	0.3	Arecibo, Goldstone	Prominent radar target.
(136617) 1994 CC	0.6	0.15	Arecibo, Goldstone, MIT	Triple system with inner/outer moons.
(153591) 2001 SN263	2.6	1	Gemini Observatory , Arecibo	Large ternary NEA system.
(175706) 1996 FG3	1.4	0.45	European Southern Observatory , Goldstone	Favorable for spin-state studies.
(363505) 2003 UC20	0.6	0.15	Arecibo, Goldstone	Radar-discovered companion.
(308635) 2005 YU55	0.4	0.1	Arecibo, Goldstone	Subject of intense flyby observations.

Observation Method	Capability & KPI Impact	Limitations
Radar Delay-Doppler	Provides line-of-sight range (distance) and velocity (Doppler frequency) with resolutions down to ~ 1.875 meters/pixel. Constrains binary orbit, sizes, spin states, and sub-surface properties.	Requires close proximity to Earth; transmitter power drops rapidly with distance (r^4 law).
Optical Astrometry	Excellent for early discoveries and measuring angular positions on the sky plane.	Poor at defining exact line-of-sight distance; uncertainties grow rapidly with time.
Optical Photometry (Lightcurves)	Determines rotation periods, binarity fractions via mutual eclipses/transits, and satellite-to-primary ratios.	Less accurate for sizing objects without albedo estimations, and does not yield precise ranging for orbit refinement.
Infrared Spectroscopy	Characterizes composition (e.g., C-class, S-class) and thermal albedo.	Provides little data on orbital dynamics, trajectories, or collision geometries.

Target Object	Estimated Diameter (km)	Radar Cross Section (RCS)	Primary Observation / Discovery Method	Key Physical KPI (Period / Density)	Associated Danger Level
66391 Moshup (1999 KW4)	1.3 (Alpha), 0.4 (Beta)	0.84 km^2	Radar Delay-Doppler & Opt	2.8h (Alpha), 17.4h (Beta) / 1.9 g/cm^3	PHA, High ΔV
80976 (2000 UQ58)	~1.2 (Alpha), ~0.4 (Beta)	~0.60 km^2	Radar Delay-Doppler	System Orbit: 12.5 days	Potentially Hazardous Asteroid (PHA)
(185851) 2000 DP107	~0.8 (Primary)	~0.30 km^2	Opt Lightcurve + Radar Delay	Orbit: 1.76 days / Dens: 1.4 g/cm^3	PHA
1994 CC	~0.6 (Primary), ~0.07 (Sec.)	~0.15 km^2	Radar delay-Doppler / Bistatic	12.2h (Pri), 27.5h (Sec) / 1.5 g/cm^3	PHA, Triple System
2003 YT1	~1.1 (Pri), ~0.15 (Sec.)	~0.55 km^2	Radar Delay-Doppler	11.9h (Pri), 36.7h (Sec) / 2.0 g/cm^3	PHA
(3122) Florence	4.5 (Primary), 0.3 (Two moons)	4.2 km^2	Optical & Radar Delay-Doppler	2.4h (Pri), 22h/27h (Moons)	PHA, Earth Close Pass

Figure 16. *a) PHA’s Detected and Observation Methods with KPI’s from Observatories i.e. Aracibo.*

Secondary diameter (D_s) refers to the physical size of the smaller, orbiting body—commonly referred to as the moonlet or satellite. secondary body (moonlet) typically has a diameter ratio of .2-.6 compared to the primary from Walsh et al. 2008 [19].

Asteroid Ephemeris Data, Orbits in the MPC

The IAU Minor Planet Center categorizes objects and issues orbital elements that can be used to generate ephemerides.

1) *Object Type Definition:* The MPC defines a "Minor Planet (Binary)" (type 1) as a "System of two asteroids orbiting their common barycenter".
2) *The Barycenter:* When dealing with two orbiting bodies of comparable or somewhat different masses (like many binary asteroids), they orbit around a common center of mass, or barycenter. For binary asteroids, this barycenter is usually located in the space between the two bodies, unlike a system with extreme mass differences (like a planet and a small satellite) where the barycenter might be inside a larger body.
3) *Orbit Basis:* The standard orbital elements provided by the MPC (like those found in the MPCORB database) typically represent the orbit of the *center of mass* (barycenter) of the entire binary system around the Sun, rather than the individual orbit of just the primary or secondary.

Generating Ephemeris Data

When calculating the ephemeris (the predicted positions over time) of a binary system, specialized tools that use MPC data handle the two bodies by referencing the main system and the specific component. Targeting the Barycenter vs. the Component: Tools like Miriade (which uses the MPCORB database) can compute the ephemeris for the system, While Miriade defaults to the ASTORB database, to generate high-precision ephemerides.

Selecting the Right Miriade Endpoint

Miriade divides its ephemeris generation into specific methods depending on the type of data required. For comprehensive asteroid analysis, three primary endpoints are used:

ephemcc (Positional Ephemerides): Generates standard astrometric positions (Right Ascension, Declination, distance) for the asteroid's barycenter.

ephemeris (Asteroid Satellites): Computes differential ephemerides for binary or multi-component systems (e.g., mapping a secondary body's orbit relative to the primary).

ephemph (Physical Ephemerides): Outputs apparent aspects, phase angles, thermal fluxes, and visual magnitudes—critical for modeling light curves and planning delay-Doppler radar imaging.

Workflow: Modeling Light Curves & Physical Properties (ephemph) To correlate time-series photometric dips with physical geometry, the ephemph endpoint computes the necessary vectors. It incorporates spin and shape models (often pulled from the DAMIT database) to provide sub-Earth point, sub-Solar point, phase angle, & magnitude.

$$R_{Primary}(t) = R_{Barycenter}(t) + r_p(t)$$

Vector Effect: The actual physical bodies are displaced by *~85.5 km* from the ephemeris coordinate, for the (The 90 Antiope System) which has 171km separation. For example, Vector Effect: The physical center of Didymos is displaced by only ~9.4 meters from the MPC ephemeris coordinate. For deep space intercept missions (like SmallSats conducting close flybys or kinetic impactors), treating the MPC ephemeris (x,y,z) as the physical target is dangerous.

2.5. ESA HERA Mission Analysis

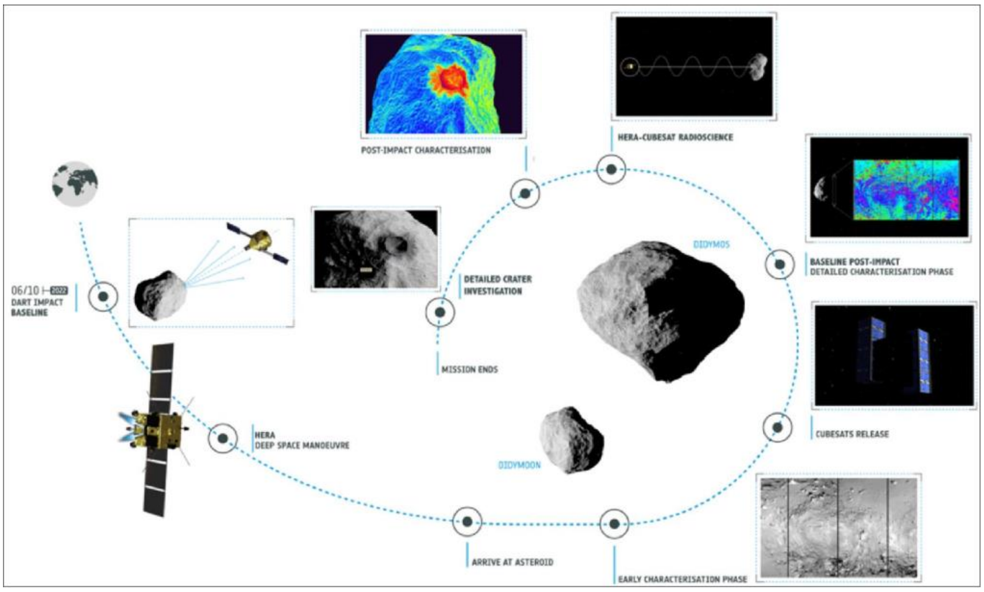

Figure 17. *Imaging and lidar surveys as well as CubeSat deployment to study the smaller of the two bodies (ESA).*

This R&D Paper Mission CONOPS POD Analysis updates $440m DART Mission Software FSW C&DH TCM Maneuvers in order to successfully image and collect data of asteroids. ESA Hera weighs ~350 kg, and up to about 870 kg full-fuelled. Its primary purpose is to refine Hera's trajectory so it precisely intersects with the Didymos system in late 2026. Propulsion System: Hera utilizes a bi-propellant chemical propulsion system consisting of 16 orbit control thrusters and 6 reaction control thrusters. ESA HERA is estimated in November 2026 for Formal Rendezvous with DART Analysis Orbit Analysis (March 2026): Findings revealed the impact shortened the orbital period of the asteroid system by approximately 33 minutes and changed the system's path around Sun by 0.15sec, confirming long-term effectiveness.

HERA Autonomous Navigation & The Image Processing Unit (IPU) Data Fusion: Hera doesn't rely entirely on the ground for deep-space routing. It navigates the low-gravity environment of the binary asteroid system using data fusion algorithms to combine readings from star trackers, inertial sensors, and lidar. HERA Inter-Satellite Links: In addition to communicating with Earth, the main flight computer manages dedicated inter-satellite radio links with two briefcase-sized CubeSats (Juventas and Milani). These mini-satellites are planned to fly closer to the surface and transmit their data back to the mothership.

HERA TCMs Aerobreaking are planned after 5.6km/sec dV before 23mo Orbit In-plane/parking angles where 3 rear thrusters align dV vector for arriving ~ Nov '26 100-1000km approaching 5m/s and ECP Arrival/Hover <30km. 12m/s Arcs down to <5-10km Detailed survey Plan. Arriving ~ Nov '26 100-1000km, with TCM2 and TCM3 60-90min small burns <5m/s for Helio cleanup, R&D may also impact TCMs 4-10 on approach & POD braking.

Data also suggests the belief of Alpha Centauri (α-Cen) A (Kentaurus) and B (Toliman) as a binary star is based on 1600s -1800s. This R&D Study expands on work from lutz, et al, 2025 how Alpha Centauri is closer to a single star system based on data analysis, angular separation, trigonometry, and image analysis [6].

3. Takeaways

1) Doppler radar, Optical lightcurves Analysis suggests potential binary orbits would not necessarily cause much change in brightness, also considering size of both rocks in comparison and % of refracted light.
2) Single vs Binary Asteroid Analysis. With 650 total binaries proposed vs 30,000 singles discovered and 1.5M single asteroids proposed, this R&D study would update asteroid databases, (MPC, JPL SSD Horizons, ASTORB, MP3C, LCDB), R&D would revise 600 asteroids identified and up to 6,000+ binaries proposed.
3) Asteroid Measurement Tools may include Reference in Image (radar, optical) to accurately determine asteroid volume-mass estimates vs V<x, y, z> as F(ε) → (n) which can be validated in space vs ground data.
4) ESA HERA $440M Mission was designed to investigate moonlet vs Didymos. This R&D Analysis may update $440m HERA Mission Software FSW, C&DH, TCM Orbits, successfully image collect data of asteroids and extend Mission CONOPs applied to other nearby asteroids objects.
5) Off-angle Data Collection with off angles >.5-2deg may be normalized with Geometric Backscatter Normalization and algorithms (such as OSOD or delay-Doppler software) with phase alignment with Python Astropy, HEASoft / NASA.

Abbreviations

AoA	Angle of Attack
C&DH	Command & Data Handling
DEC	Declination
DDM	Delay-Doppler Map (DDM)
DDM	Flight Software
FSW	Flight Software
IAU	International Astronautical Union
NEA	Near Earth Asteroid
OTH	Over-the-Horizon
TCM	Trajectory Correction Maneuvers

Acknowledgments

Author K. Lutz thanks friends and family and MPU University and Magneto Space for helping sustain research. The authors confirm this material or similar material has not been published in any other publication.

Author Contributions

Kolemann Lutz: Conceptualization, Data curation, Formal Analysis, Investigation, Methodology, Resources, Writing – review & editing

Data Availability Statement

The data supporting the outcome of this research work has been reported in this manuscript. The data is available from the corresponding author upon reasonable request.

Conflicts of Interest

The authors declare no conflicts of interest and no competing financial interests.

References

[1] Ferrari, F., Panicucci, P., Merisio, G. et al. Morphology of ejecta features from the impact on asteroid Dimorphos. Nat Commun 16, 1601 (2025). https://doi.org/10.1038/s41467-025-56551-0

[2] Graykowski, et al, 2023. Light curves and colours of the ejecta from Dimorphos after the DART impact. Nature 616, 461–464 (2023). https://doi.org/10.1038/s41586-023-05852-9

[3] Hickson, D. C., et al (2020). Modeling the dielectric properties of minerals from crystals to bulk powders for improved interpretation of asteroid radar observations. *Journal of Geophysical Research: Planets*, 125, e2019JE006141. https://doi.org/10.1029/2019JE006141

[4] Johnston, 2026, Asteroids with Satellites by Wm. Robert Johnston last updated 11 June 2026, https://www.johnstonsarchive.net/astro/asteroidmoons.html

[5] Li, JY., Hirabayashi, M., Farnham, T. L. et al. Ejecta from the DART-produced active asteroid Dimorphos. Nature 616, 452–456 (2023). https://doi.org/10.1038/s41586-023-05811-4

[6] Lutz, K. (2025). Alpha Centauri Not a Binary Star System, Angular Separation, Brightness Analysis. International Journal of Astrophysics and Space Science, 13(2), 63-72. https://doi.org/10.11648/j.ijass.20251302.14

[7] Lutz, 2026. "Cubesat Missions, Build, Payload Systems, AIT To Operate Spacecraft in Orbits," AIAA 2026-3033. ASCEND 2026. May 2026. https://doi.org/10.2514/6.2026-3033

[8] Moskovitz, N. A., et al (2023). Photometry of the Didymos System across the DART Impact Apparition. The Planetary Science Journal, 5. https://doi.org/10.3847/PSJ/ad0e74

[9] Naidu, et al (2024). Orbital and Physical Characterization of Asteroid Dimorphism Following the DART Impact. The Planetary Science Journal. 5. 74. https://doi.org/10.3847/PSJ/ad26e7

[10] Naidu, et al, 2020. Radar observations and a physical model of binary near-Earth asteroid 65803 Didymos, target of the DART mission, Icarus, Volume 348, 2020, 113777, https://doi.org/10.1016/j.icarus.2020.113777

[11] Naidu, Shantanu & Chesley, Steven & Farnocchia, Davide & Moskovitz, Nick & Pravec, Petr & Scheirich, Peter & Thomas, Cristina & Rivkin, Andrew. (2022). Anticipating the DART impact: Orbit estimation of Dimorphos using a simplified model. https://doi.org/10.48550/arXiv.2210.05101

[12] NASA CNEOS, NASA’s DART Mission Changed Orbit of Asteroid Didymos Around Sun, March 6, 2026.

[13] Ostro, S. & Hudson, Scott & Benner, L. & Giorgini, J. & Magri, C. & Margot, J. & Nolan, Michael. (2002). Asteroid Radar Astronomy. Asteroids III.

[14] Rahil Makadia et al. 2026, Direct detection of an asteroid’s heliocentric deflection: The Didymos system after DART. Sci. Adv.12, eaea4259(2026). https://doi.org/10.1126/sciadv.aea4259

[15] Scheirich et al 2024. The Planetary Science Journal, 5(1), 17 (2024), Published by the American Astronomical Society. https://doi.org/10.48550/arXiv.2403.02804

[16] Shantanu P. Naidu et al 2022, Anticipating the DART Impact: Orbit Estimation of Dimorphism Using a Simplified Model, Planet. Sci. J. 3 234, https://iopscience.iop.org/article/10.3847/PSJ/ac91c0

[17] Shepard, M. K., 2015 “A radar survey of M- and X-class asteroids. III. Insights into their composition, hydration state, & structure”, Icarus Elsevier, pp. 38–55, 2015. https://doi.org/10.1016/j.icarus.2014.09.016

[18] Virkki, et al (2022). Arecibo Planetary Radar Observations of Near-Earth Asteroids: 2017 December–2019 December. The Planetary Science Journal. 3. 222. https://doi.org/10.3847/PSJ/ac8b72

[19] Walsh, and Richardson, 2008, A steady-state model of NEA binaries formed by tidal disruption of gravitational aggregates, Icarus, Volume 193, Issue 2, 2008, Pages 553-566, ISSN 0019-1035, https://doi.org/10.1016/j.icarus.2007.08.020

[20] Whittaker, 2020, uncertainty assessment of near-earth asteroid size measurements from radar images, 51st Lunar and Planetary Science Conference (2020), https://www.hou.usra.edu/meetings/lpsc2020/pdf/1446.pdf

[21] Kikuchi, 2019, Asteroid de-spin and deflection strategy using a solar-sail spacecraft with reflectivity control devices, Acta Astronautica, Volume 156, 2019, Pages 375-386, ISSN 0094-5765, https://doi.org/10.1016/j.actaastro.2018.06.047

[22] Nath, A. (2024). Algorithms to Determine Asteroid's Physical Properties using Sparse and Dense Photometry, Robotic Telescopes and Open Data. SciPy. https://doi.org/10.25080/TWCF2755

[23] Chen, X., Li, G., Chen, Z., Ju, Q., & Cheng, X. (2022). Incidence Angle Normalization of Dual-Polarized Sentinel-1 Backscatter Data on Greenland Ice Sheet. Remote Sensing, 14(21), 5534. https://doi.org/10.3390/rs14215534

[24] Kunduri, B. S. R., Baker, J. B. H., Ruohoniemi, J. M., Thomas, E. G., & Shepherd, S. G. (2022). An examination of SuperDARN backscatter modes using machine learning guided by ray-tracing. Space Weather, 20, e2022SW003130. https://doi.org/10.1029/2022SW003130

[25] Topouzelis, Konstantinos, Singha, Suman and Kitsiou, Dimitra. "Incidence angle normalization of Wide Swath SAR data for oceanographic applications" Open Geosciences, vol. 8, no. 1, 2016, pp. 450-464. https://doi.org/10.1515/geo-2016-0029

[26] Li, Xinghua & Feng, Ruitao & Guan, Xiaobin & Shen, Huanfeng & Zhang, Liangpei. (2019). Remote Sensing Image Mosaicking: Achievements and Challenges. IEEE Geoscience and Remote Sensing Magazine. 7. 8-22. https://doi.org/10.1016/B978-0-44-343796-0.00012-7

Biography

Kolemann Lutz is a researcher with 6+ years in R&D, physics, materials, space, astrophysics, and math. He has published 25+ research publications to advance physics, biology, engineering, & life on Earth, in space, and beyond. He is the Cofounder and Faculty of Multiplanet University. In co-founding MPU in 2020, Kolemann has led a team of 20+ staff, faculty and researchers. He is an alumni from ISU in Space Systems Engineering in 2020, graduated with a Bachelors of Science from University of Mary Washington (UMW) in 2017, and studied physics from several universities UVA & UMW. He was recently awarded Top 100 Men in Aerospace in 2022 and is a Lead Scientist and PI with proposed NASA Projects and Missions.

Research Field

Kolemann Lutz: Earth, Planetary Space Sciences, Physics, applied mathematics, electromagnetism, Astrophysics, Heliophysics, Aerospace Systems, Materials Science and Engineering